



ELSEVIER

Contents lists available at ScienceDirect

## Journal of Magnetism and Magnetic Materials

journal homepage: [www.elsevier.com/locate/jmmm](http://www.elsevier.com/locate/jmmm)

## Research articles

Tunable K vacancies in  $K_{1-x}Co_2Se_2$  and their effects on structure and ferromagnetism

Zhongnan Guo<sup>a</sup>, Xiaoxiao Yan<sup>a</sup>, Lirong Zheng<sup>b</sup>, Xue Han<sup>a</sup>, Dan Wu<sup>a</sup>, Ning Liu<sup>c</sup>, Fan Sun<sup>a</sup>, Da Wang<sup>c</sup>, Wenxia Yuan<sup>a,\*</sup>

<sup>a</sup> Department of Chemistry, School of Chemistry and Biological Engineering, University of Science and Technology Beijing, Beijing 100083, China

<sup>b</sup> Beijing Synchrotron Radiation Facility, Institute of High Energy Physics, Chinese Academy of Sciences, Beijing 100049, China

<sup>c</sup> Research & Development Center for Functional Crystals, Beijing National Laboratory of Condensed Matter Physics, Institute of Physics, Chinese Academy of Sciences, Beijing 100190, China

## ARTICLE INFO

## Keywords:

KCo<sub>2</sub>Se<sub>2</sub>ThCr<sub>2</sub>Si<sub>2</sub>-type structure

K vacancies

Ferromagnetism

## ABSTRACT

Deeply understanding the role of intermediate metal *A* on structure and related properties of ThCr<sub>2</sub>Si<sub>2</sub>-type transition metal compounds  $ATM_2X_2$  is of great importance for designing novel layered functional materials. However, inducing *A* vacancies usually trends to destroy the original structure in reported systems so far, which hampers the further research. Here we report the controllable K vacancies in  $K_{1-x}Co_2Se_2$  system ( $0 \leq x \leq 0.3$ ), where both the ThCr<sub>2</sub>Si<sub>2</sub>-type structure and intact tetrahedral [CoSe] layers can be maintained with the varying occupancies of K. By inducing K vacancies in structure, tetragonality of the lattice for  $K_{1-x}Co_2Se_2$  increases with the shortened *a* and elongated *c*. The (CoSe<sub>4</sub>) tetrahedron is also compressed perpendicular to the *c* direction resulted from the K deficiency. X-ray absorption near-edge structure reveals that the valence state of Co is basically unaffected by K deficient with the absorption edge of Co K-edge unchanged. Concerning the physical properties, K vacancies increase the resistivity of metallic  $K_{1-x}Co_2Se_2$  due to the decreased charge transfer from K<sup>+</sup> to [CoSe] layers. More importantly, the ferromagnetic interaction of  $K_{1-x}Co_2Se_2$  is unexpectedly weakened by raising K vacancies with the Curie temperature shifted from 80 to 52 K, despite the shortened Co-Co distance. First-principles calculation reveals that the spin polarization is weakened resulted from the K vacancies, mainly attributed to the reduced charge transfer from K<sup>+</sup> to [CoSe] host. Our results clearly indicate the domination of transferred electrons from intermediate metal *A* on the magnetic interaction of  $ATM_2X_2$ , and also show the feasibility to regulate the structure and related properties of  $ATM_2X_2$  by controlling the *A* content.

## 1. Introduction

Layered transition metal chalcogenides/arsenides  $ATM_2X_2$ , which contain the intermediate metal (*A* = alkalis, alkali earths or lanthanides) between [TMX] host layers (*TM* = transition metals, and *X* = S, Se, P or As), usually crystallize with the ThCr<sub>2</sub>Si<sub>2</sub>-type structure in a body-centered tetragonal lattice (space group: *I4/mmm*) [1–3]. Due to the *d* electrons from transition metal,  $ATM_2X_2$  exhibits very rich electromagnetic properties, such as high-temperature superconductivity [4,5], interlayer magnetic interaction [6], and heavy fermion behaviour [7] as well. From the structure point of view, the covalent bonded [TMX] layers adopt fluorite structure with edge-sharing (TMX<sub>4</sub>) tetrahedrons and act as the functional layers. It is believed that the properties of these materials are originated from [TMX], mainly determined by the species of transition metals [3]. The intermediate metals *A*,

considered as the guest species, also play an important role in regulating the properties of  $ATM_2X_2$  since the electrons can easily transfer from intermediate metals to the host. It has been reported that the superconducting critical temperature can be adjusted from 18 to 46 K in Fe selenides by changing the intermediate metals [8–10], and the magnetic interaction ordering can also be modulated (from ferromagnetic to anti-ferromagnetic) by adopting different *A* in layered Co arsenides [11–14].

Charge transfer from intermediate metals *A* is highly relevant to the electronic structure of  $ATM_2X_2$ . Inducing the vacancies at *A* sites can give rise to the adjustment of carrier concentration in [TMX] layers, leading to the regulation on related electromagnetic properties. Compared with the vacancies at *TM* sites which generally destroy the related feature [15,16], tunable *A* vacancies in  $ATM_2X_2$  are expected to be more gentle and effective to modulate the related properties since

\* Corresponding author.

E-mail address: [wxyuanwz@163.com](mailto:wxyuanwz@163.com) (W. Yuan).

<https://doi.org/10.1016/j.jmmm.2019.165473>

Received 6 December 2018; Received in revised form 9 April 2019; Accepted 18 June 2019

Available online 19 June 2019

0304-8853/© 2019 Published by Elsevier B.V.

the [TMX] host would be maintained and intact. Consequently, a deep understanding on this regulation will be of great help for the material design in  $ATM_2X_2$  system. However, tuning the A vacancies in  $ATM_2X_2$  trends to be unattainable in arsenides due to the request of valence balance from the negative [TMAs]<sup>-</sup> [17,18]. For TM chalcogenides with electrically neutral [TMX], the deficient A was reported to reduce the structural stability in Ni-based system, leading to the collapse of ThCr<sub>2</sub>Si<sub>2</sub>-type structure [19]. These issues hinder us to thoroughly understand the regulation of intermediated metal A on the structure and related properties of  $ATM_2X_2$ . In order to solve this problem, a system where the content of intermediate metal A can be easily controlled without inducing any TM vacancy or structural instability is required.

Layered cobalt selenide KCo<sub>2</sub>Se<sub>2</sub> with ThCr<sub>2</sub>Si<sub>2</sub>-type structure was reported to show A-type ferromagnetism [6]. Wide investigations have been done on KCo<sub>2</sub>Se<sub>2</sub> and its sister compounds ACo<sub>2</sub>Ch<sub>2</sub> (A = Rb, Cs, Tl and Ch = Se, S) by chemical doping on A, Co and Ch sites, leading to a series of novel magnetic phase transitions [20–25]. However, the effort to adjust the A vacancies in these layered Co selenides has not been reported. In this work, we report the intrinsic feature of tunable K vacancies in nominal K<sub>1-x</sub>Co<sub>2</sub>Se<sub>2</sub> (0 ≤ x ≤ 0.3). It is indicated that both the ThCr<sub>2</sub>Si<sub>2</sub>-type structure and intact [CoSe] layers can be well maintained when the composition of intermediate metal is adjusted in this system. With the K vacancies increased, the lattice parameter *a* is shortened while *c* is elongated, resulting in an increased tetragonality (*c/a*). Concerning physical properties, K vacancies significantly increases electric resistivity of K<sub>1-x</sub>Co<sub>2</sub>Se<sub>2</sub> by reducing the transferred electrons. More interestingly, in spite of the shortened Co-Co distance in [CoSe] functional layers, inducing the K vacancies leads to weaker magnetic interaction with Curie temperature (*T<sub>C</sub>*) of K<sub>1-x</sub>Co<sub>2</sub>Se<sub>2</sub> decreased from 80 to 52 K. This suggests that the ferromagnetic interaction in K<sub>1-x</sub>Co<sub>2</sub>Se<sub>2</sub> is mainly governed by the charge transfer, rather than the structural parameters. First-principle calculation is also carried out to explore the mechanism of these effects from K vacancies.

## 2. Experimental

### 2.1. Synthesis

The polycrystalline samples K<sub>1-x</sub>Co<sub>2</sub>Se<sub>2</sub> (with *x* = -0.2, 0, 0.1, 0.2, 0.3, 0.4 and 0.5) were synthesized by solid state reaction. Powders of Co (99.8%) and Se (99.95%) obtained from Alfa Aesar were mixed and ground in an agate mortar, followed by cold-pressing into disks (1 mm in diameter) with a 200 kg/cm<sup>2</sup> uniaxial stress. The disks were put into the alumina crucibles together with the cut K ingot (97%, from China National Accord Medicines Corporation) with predetermined compositions and sealed into quartz tubes under vacuum (10<sup>-2</sup> mbar). The tubes were heated to 473 K with the heating rate of 100 K/h, held for 12 h and then to 973 K for 48 h to obtain the precursors. After grinding, the samples were re-heated at 923 K for 72 h to obtain the homogeneous phase and then cooled down to room temperature by turning off the furnace. All manipulations for sample preparation were carried out inside an argon-filled glove box (O<sub>2</sub> < 1 ppm) in order to prevent the oxidation.

### 2.2. Characterization

Powder X-ray diffraction (PXRD) of the nominal samples K<sub>1-x</sub>Co<sub>2</sub>Se<sub>2</sub> were collected at room temperature on a PANalytical diffractometer (X'Pert PRO MRD) equipped with CuKα radiation (λ = 1.5148 Å) operation at 40 kV and 40 mA and a diffracted-beam graphite monochromator in a reflection mode (step = 0.017°2θ, scan speed = 0.07 s/step for phase define and 0.47 s/step for structure analysis). Temperature-dependent in situ PXRD was performed at 200 and 100 K by using a Rigaku SmartLab SE instrument (CuKα radiation) equipped with an Anton Paar nonambient sample stage. Rietveld refinements were performed using the FULLPROF package [26]. The

stoichiometric KCo<sub>2</sub>Se<sub>2</sub> structure was used as the starting model to refine the K<sub>1-x</sub>Co<sub>2</sub>Se<sub>2</sub> samples with *x* = 0, 0.1, 0.2 and 0.3. The morphology of samples was investigated via scanning electron microscopy (SEM, Hitachi S-4800) and transmission electron microscopy (together with the selected area electron diffraction (SAED)) (TEM, JEOL JEM-2100F). The component analysis of Co, Se and K was made by energy dispersive X-ray spectroscopy (EDS). The result for each sample was obtained based on the average of 7–10 sets of data. The valence state of Co was investigated by X-ray absorption fine structure (XAFS) which was collected on the 1W1B beamline at Beijing Synchrotron Radiation Facility (BSRF). The samples were recorded at the Co K-edge (*E*<sub>0</sub> = 7709 eV) at room temperature. The magnetization susceptibility was measured by using a vibrating sample magnetometer (VSM, Quantum Design). The electrical resistivity was measured with the cold-pressed samples under a uniaxial stress of 600 kg·cm<sup>-2</sup> via a typical four-probe method on physical property measurement system (PPMS).

### 2.3. First-principles calculation

Electronic structure calculations were performed using the CASTEP program with plane-wave pseudopotential method [27]. Generalized gradient approximation (GGA) in the form of the Perdew-Burke-Ernzerhof was chosen to solve the exchange-correlation potentials. The ultrasoft pseudopotential with a plane-wave energy cutoff of 330 eV and a Monkhorst Pack *k*-point separation of 0.04 Å<sup>-1</sup> in the reciprocal space were used for all the calculations [28]. The self-consistent field was set as 10<sup>-6</sup> eV/atom. A 2 × 2 × 1 supercell with Co vacancy sites was built to simulate the K<sub>0.75</sub>Co<sub>2</sub>Se<sub>2</sub> with 25% K vacancies.

## 3. Results and discussion

The obtained K<sub>1-x</sub>Co<sub>2</sub>Se<sub>2</sub> samples are dark microcrystalline solids, which are unstable to air and moisture. So the samples were kept in the glove box before they were mounted for characterization. Fig. 1 shows the PXRD patterns for a series of K<sub>1-x</sub>Co<sub>2</sub>Se<sub>2</sub> with nominal *x* = -0.2, 0, 0.1, 0.2, 0.3, 0.4 and 0.5 collected at room temperature. The main phase of each pattern can be well indexed by the body-centered tetragonal cell with space group *I4/mmm* (No. 139). For sample with excess K (*x* = -0.2) an impurity marked by # is assigned to K<sub>2</sub>CoSe<sub>2</sub> (ICSD PDF: 79–2149). And for samples with *x* = 0.4 and 0.5, binary CoSe (ICSD PDF: 70–2870) was observed, marked by asterisk. It can be seen that the impurity CoSe also arises in sample with *x* = 0.3 but with a very small amount. For samples with *x* = 0, 0.1 and 0.2, pure phase can be obtained. It suggests that the K<sub>1-x</sub>Co<sub>2</sub>Se<sub>2</sub> shows solid solution respect to K content with the boundary around *x* = 0.3. This solid solution could be further confirmed by the inset of Fig. 1, where the (0 0 2) and (2 0 0) peaks gradually shift to lower and higher 2θ angles respectively with the nominal *x* increased from 0 to 0.3.

Rietveld refinements were carried out on PXRD patterns of samples with *x* = 0–0.3 to solve the structure of these tetragonal phases. A typical refinement of sample *x* = 0.3 is plotted in Fig. 2a, showing a satisfactory level for fitting the experimental pattern. All the obtained structural parameters are listed in Table 1. It needs to be mentioned that only sample *x* = 0.3 contains 6.6 at.% CoSe, while the other three show no diffraction peak from any impurity. The K-site occupations for different samples show significant deviation from each other, varying from 0.98(1) (*x* = 0) to 0.69(1) (*x* = 0.3). On the contrary, both Co and Se sites are fully occupied. So it is indicated that the vacancies of K are tunable in this ThCr<sub>2</sub>Si<sub>2</sub>-type compound with maximum content ~30% (Fig. 2b). The observation of hexagonal CoSe impurity in sample *x* = 0.3 could be mainly resulted from the loss of alkali metal during the sample preparation, which leads to less K content in the reaction. EDS measurements were used to confirm the variation of K content in these samples and the measured chemical compositions of sample *x* = 0, 0.1, 0.2 and 0.3 are K<sub>1.02</sub>Co<sub>1.96</sub>Se<sub>2</sub>, K<sub>0.87</sub>Co<sub>2</sub>Se<sub>2</sub>, K<sub>0.76</sub>Co<sub>1.98</sub>Se<sub>2</sub> and K<sub>0.67</sub>Co<sub>2.01</sub>Se<sub>2</sub> respectively, which are comparable to our refinements. A

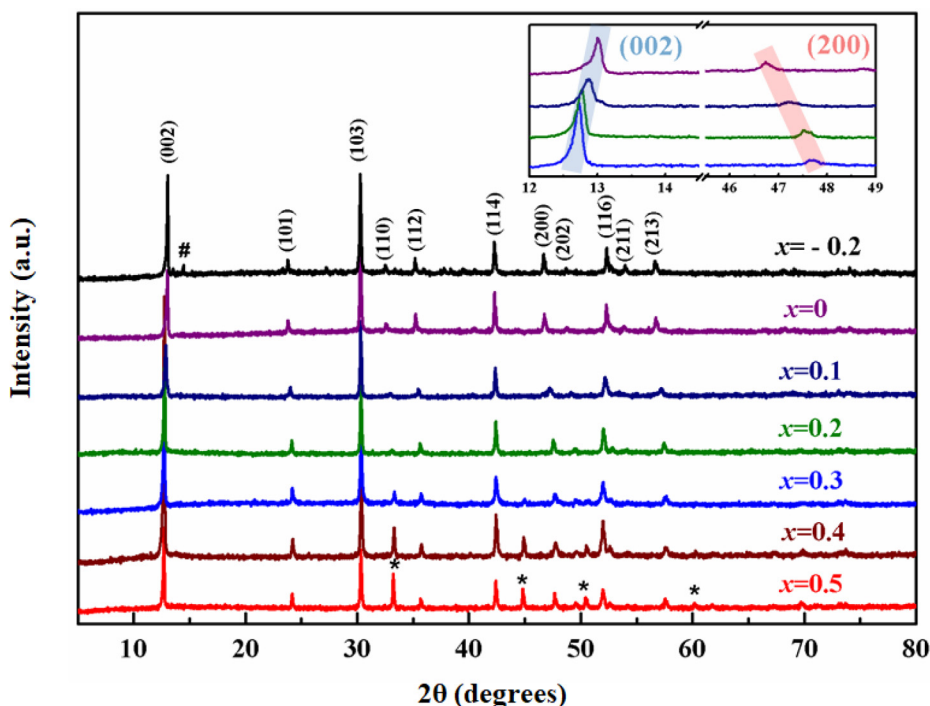


Fig. 1. PXPD patterns for nominal  $K_{1-x}Co_2Se_2$  ( $x = -0.2, 0, 0.1, 0.2, 0.3, 0.4$  and  $0.5$ ). The reflections marked by (\*) and (#) are assigned to hexagonal CoSe and  $K_2CoSe_2$ , respectively. Sample with  $x = -0.2$  represents the nominal composition  $K_{1.2}Co_2Se_2$ . Inset shows the enlarged (002) and (200) peaks of  $K_{1-x}Co_2Se_2$ , and the blue and red area are eye guide for peak shifting. (For interpretation of the references to colour in this figure legend, the reader is referred to the web version of this article.)

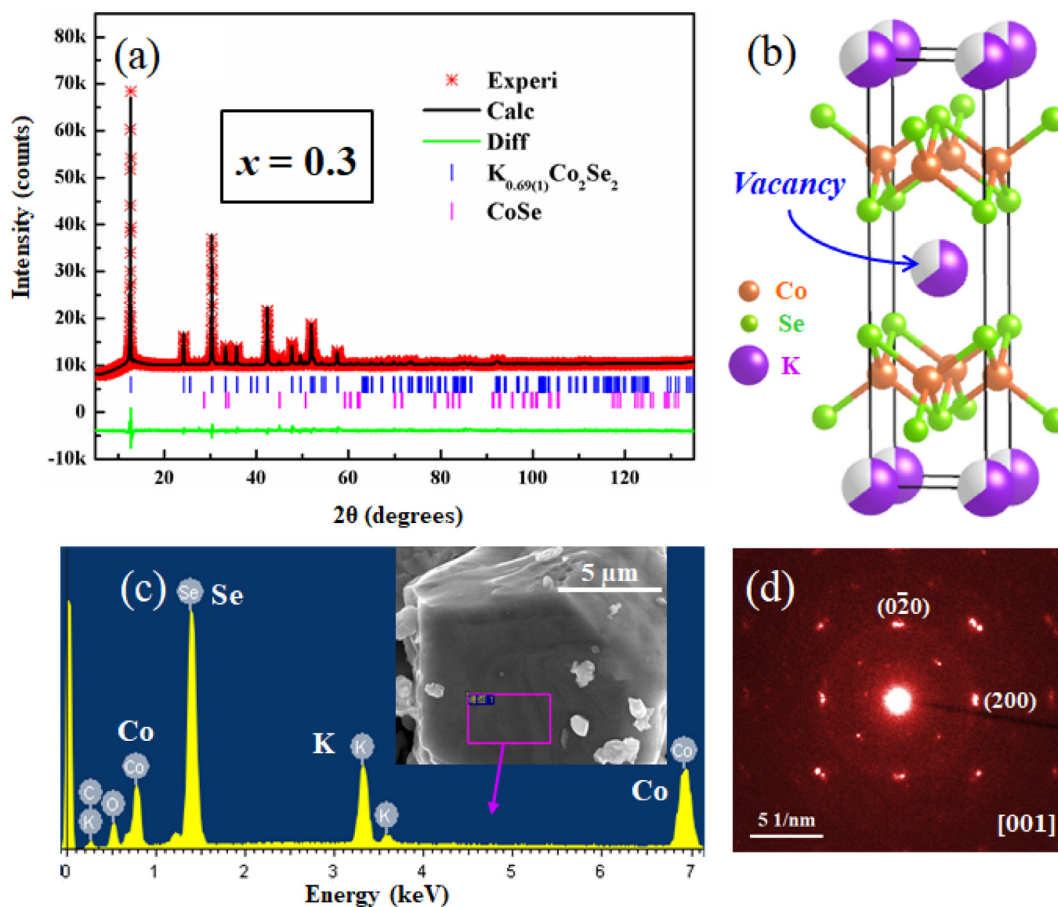
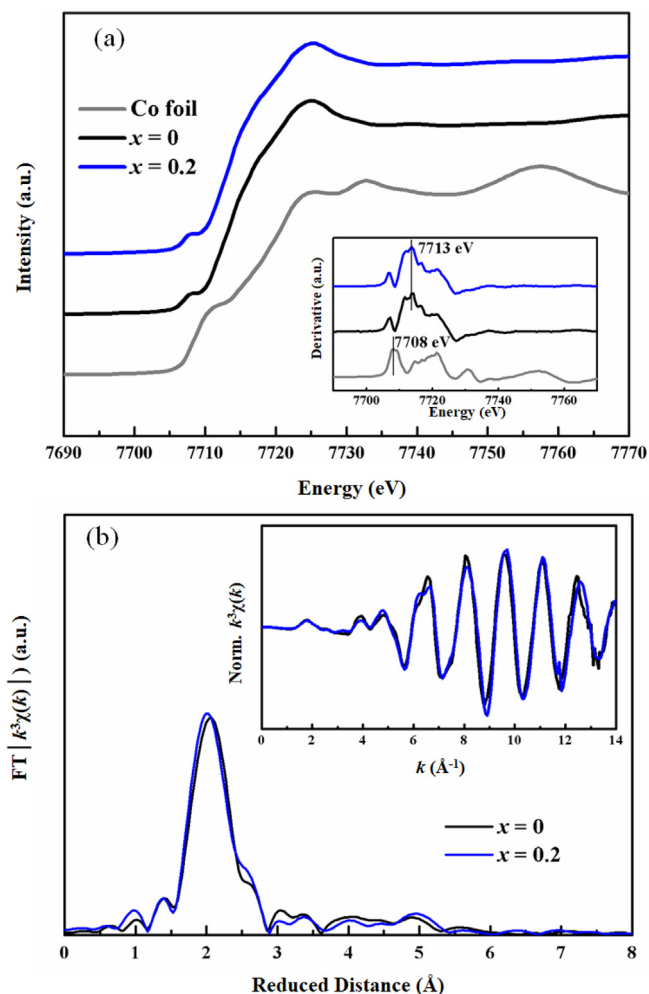


Fig. 2. (a) PXPD pattern for nominal  $K_{0.7}Co_2Se_2$  (the sample with  $x = 0.3$ ) with the final Rietveld refinement. (b) Crystal structure for  $K_{0.7}Co_2Se_2$  with deficient K in the lattice. (c) EDS spectrum for  $K_{0.7}Co_2Se_2$  with the electronic microscope photograph of a crystal particle inset. (d) SAED pattern for  $K_{0.7}Co_2Se_2$ .

**Table 1**  
Refinement parameters for nominal  $K_{1-x}Co_2Se_2$  ( $x = 0, 0.1, 0.2$  and  $0.3$ ).

Nominal	$x = 0$	$x = 0.1$	$x = 0.2$	$x = 0.3$
Refined	$K_{0.98(1)}Co_2Se_2$	$K_{0.85(1)}Co_2Se_2$	$K_{0.78(1)}Co_2Se_2$	$K_{0.69(1)}Co_2Se_2$
$a$ (Å)	3.8832(3)	3.8520(4)	3.8233(3)	3.8117(4)
$c$ (Å)	13.5941(7)	13.7520(8)	13.8601(6)	13.9145(8)
$\alpha_{Se-Co-Se}$ (°)	109.18(8)	107.18(8)	106.80(8)	106.38(9)
$\beta_{Se-Co-Se}$ (°)	110.06(9)	110.63(8)	110.82(8)	111.04(9)
Co-Se (Å)	2.3694(16)	2.3932(14)	2.3812(15)	2.3804(17)
$R_{wp}$ (%)	2.15	2.54	3.02	3.83
$\chi^2$	2.95	5.21	4.49	3.62



**Fig. 3.** (a) The Co  $K$ -edge XANES spectra of Co foil,  $KCo_2Se_2$  ( $x = 0$ ) and  $K_{0.8}Co_2Se_2$  ( $x = 0.2$ ). Inset shows the first-derivatives of the XANES spectra. (b) Fourier transform (FT) of the Co  $K$ -edge EXAFS  $k^3\chi(k)$  functions for  $KCo_2Se_2$  and  $K_{0.8}Co_2Se_2$ . The inset displays their normalized EXAFS  $k^3\chi(k)$  functions.

typical result of sample with  $x = 0.3$  is shown in Fig. 2c. Both Rietveld refinement and EDS exclude the existence of obvious Co deficiency in the series of samples. Hence, we indicate that the [CoSe] layers are intact in this system when K vacancies are induced in the structure. To further reveal the microstructure features of  $K_{1-x}Co_2Se_2$ , SAED investigation was also carried out on the sample with  $x = 0.3$  and as shown in Fig. 2d, the diffraction spots can be well indexed by  $I4/mmm$  space group, which is in agreement with the PXRD pattern. It is worth noting that no superstructure has been found, because no extra spot besides the ones from tetragonal lattice was observed. It suggests that the K vacancies in  $K_{1-x}Co_2Se_2$  system are totally disordered.

The X-ray absorption fine structure (XAFS) spectra of samples  $x = 0$

and 0.2 were also collected at room temperature and plotted in Fig. 3a together with that of Co foil as reference. It can be seen that the Co  $K$ -edge X-ray absorption near-edge structure (XANES) spectra of  $KCo_2Se_2$  and  $K_{0.8}Co_2Se_2$  are basically the same, but obviously different from that of Co foil. A weak pre-edge feature around 7708 eV can be observed, which is attributed to  $1s \rightarrow 3d$  transition of transition metal [29]. Meanwhile, both two curves show a strong asymmetrical absorption located at around 7725 eV, corroborating the high-spin  $Co^{2+}$  ions in tetrahedral coordination in two samples (the absorption of octahedral  $Co^{3+}$  ions is located around 7729 eV, as reported in literatures) [30,31]. Comparing with the data from literature [32],  $K_{1-x}Co_2Se_2$  system shows very similar spectra with that of CoO, implying the oxide state in our sample is close to +2. The first-derivatives of XANES spectra inset show the absorption edges of Co  $K$ -edge for  $KCo_2Se_2$  and  $K_{0.8}Co_2Se_2$  are located at 7713 eV. This suggests that the K vacancies in structure hardly affect the Co valence state. Additionally, the Co  $K$ -edge extended XAFS (EXAFS)  $k^3\chi(k)$  functions of  $KCo_2Se_2$  and  $K_{0.8}Co_2Se_2$  are basically the same (inset of Fig. 3b), and the Fourier transform (FT) of EXAFS of two samples are also similar, both showing a single peak (Fig. 3b). This clearly validates that the K vacancies do not break the  $(CoSe_4)$  tetrahedron in  $K_{1-x}Co_2Se_2$ .

It is suggested that a certain amount of K is still requested to stabilize the  $ThCr_2Si_2$ -type structure during high-temperature synthesis, which is  $\sim 70\%$  based on our work. Recently, Zhou et al reported the synthesis of binary tetrahedral CoSe by de-intercalating K from  $KCo_2Se_2$  precursor at room temperature, where the product is metastable in thermodynamics [33]. This implies that the content of K vacancies might be tuned in a wider range ( $> 30\%$ ) through low-temperature synthesis. Although the regulating composition of K in  $K_{1-x}Co_2Se_2$  is limited here, the high-temperature route used in our work can realize much better crystalline and even large-size single crystals. On the other hand, our attempt to introduce K vacancies in  $KCo_2Se_2$  by solid state reaction was failed. We speculate that the suitable lattice parameters in  $ATM_2X_2$  system could also be a critical factor for the tunable vacancy of intermediate metal A, since  $KCo_2Se_2$  is simply the isologous of  $KCo_2Se_2$  with compressed lattice.

Based on the tunable K vacancies in  $K_{1-x}Co_2Se_2$ , we could make a thorough analysis of the influence of intermediate metal A on structure parameters of this  $ThCr_2Si_2$ -type phase. The lattice constants and two Se-Co-Se angles in  $K_{1-x}Co_2Se_2$  depended on the refined vacancy content  $x$  are schematized in Fig. 4. The obtained parameters of stoichiometric  $KCo_2Se_2$  are comparable with the reported data [6]. By increasing  $x$  to 0.3,  $a$  axis is significantly shortened from 3.8832(3) to 3.8117(4) Å, suggesting that the covalent bonding in [CoSe] host layers is strengthened due to the induced K vacancies. On the contrary,  $c$  axis lengthens from 13.5941(7) to 13.9145(8) Å with the reduced K composition. This can be explained by a smaller Coulomb force between [CoSe] functional layers caused by less  $K^+$  cations [9,34]. Meanwhile, the varying K content also leads to the distortion of  $(CoSe_4)$  tetrahedron. In stoichiometric  $KCo_2Se_2$ , the tetrahedrons are slightly distorted from the perfect (Se-Co-Se angle =  $109.47^\circ$ ) with  $\alpha = 109.18(8)^\circ$  and  $\beta = 110.06(9)^\circ$ . With vacancies increased, the distortion is clearly exacerbated with the difference between  $\alpha$  and  $\beta$  getting larger (lower part of Fig. 4). This suggests that the K deficiency also drives a compression on  $CoSe_4$  tetrahedrons along the  $ab$  plane. It has been reported that in tetragonal CoSe (which can be considered as the  $K_{1-x}Co_2Se_2$  with  $x = 1$ ) this distortion is  $\alpha = 105.8(2)^\circ$  and  $\beta = 111.382(63)^\circ$  [33], which is in line with the tendency from our results [35].

Temperature-dependent in situ PXRD was also performed at 200 and 100 K for sample  $x = 0$  and  $x = 0.2$ , to further investigate the structure in low temperature range. As shown in Fig. 5, the  $I4/mmm$  space group is maintained at 200 and 100 K for both two samples, with no extra diffraction peak observed besides the one from the tetragonal lattice. The enlarged (1 0 3) diffraction peaks do not split off, suggesting that there is no decreased symmetry occurred in this Co-based system. Hence, it is indicated that there is not any structure distortion or phase

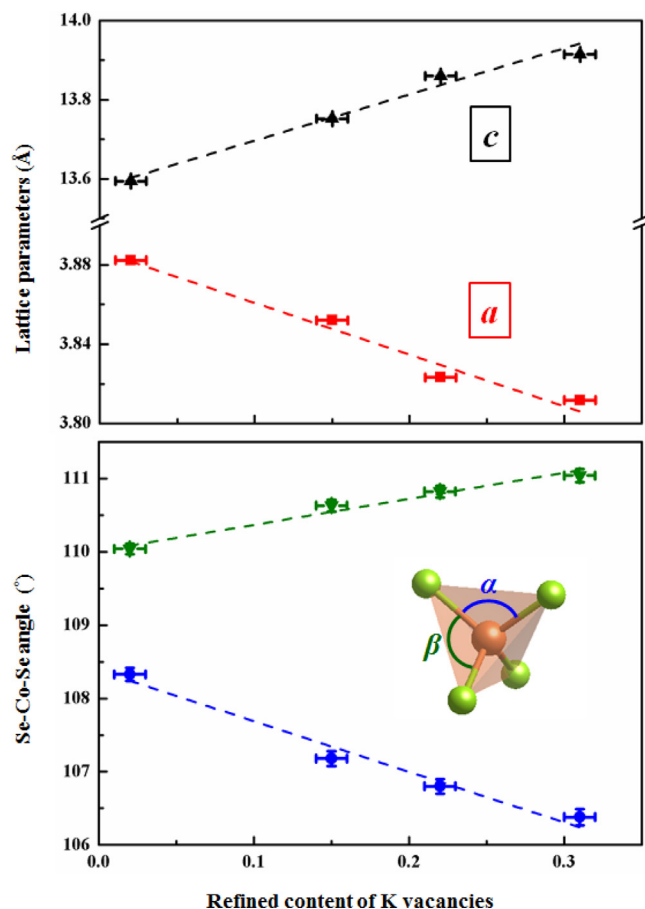


Fig. 4. Lattice parameters  $a$ ,  $c$  (upper) and two Se-Co-Se angles (lower) as a function of refined K vacancy contents in  $K_{1-x}Co_2Se_2$ .

transition in  $K_{1-x}Co_2Se_2$  system from room temperature down to 100 K. By indexing the patterns, the lattice parameter  $a$  for  $K_{0.8}Co_2Se_2$  at 100 K (3.8013(3) Å) is still smaller than that of the stoichiometric  $KCo_2Se_2$  (3.8356(4) Å), showing the shorter Co-Co distance in  $ab$  plane in this K deficient phase even in the low temperature range.

The temperature-dependent resistivity of  $K_{1-x}Co_2Se_2$  shown in Fig. 6 exhibits the metallic behavior in measured temperature range from 300 and 5 K with the resistivity of all samples below 3 mΩ·cm at room temperature. It is noted that with the increased K vacancies, resistivity increases with the data of sample  $x = 0.3$  a fifth larger than that of  $x = 0$ . This could be easily understood since the intermediate metal K in this system plays the key role for charge transfer to [CoSe] host layers. Increasing the K vacancies would certainly reduce the carrier concentration in  $K_{1-x}Co_2Se_2$ , hence enhance the electric resistivity.

Fig. 7 shows the temperature dependence of magnetic susceptibility  $\chi$  of  $K_{1-x}Co_2Se_2$ . All the curves clearly show the ferromagnetic ordering behavior below 100 K. It should be mentioned that the existence of impurity phase in sample  $x = 0.3$  does not interfere with the ferromagnetic transition, since the hexagonal CoSe is reported to be paramagnetic [36]. With the K vacancies increased, the ferromagnetic interaction is weakened with the Curie temperature  $T_C$  decreased from 80 K for  $x = 0$ , to 67, 56 and 52 K for  $x = 0.1, 0.2$  and  $0.3$  respectively ( $T_C$ s were obtained from the derivative susceptibility [15]). The hysteresis loops at 10 K shown in Fig. 8 confirm the ferromagnetism in  $K_{1-x}Co_2Se_2$  system and also indicate that the samples are soft ferromagnets according to the weak hysteresis (inset of Fig. 8). From Fig. 8a, the saturated magnetic moment for stoichiometric  $KCo_2Se_2$  is 0.73  $\mu_B/Co$ , which is consistent with the value reported in literature (0.75  $\mu_B/Co$ ) [23]. As the K vacancies involved, the moments at 4 T are reduced

to 0.65, 0.46 and 0.32  $\mu_B/Co$  for samples  $x = 0.1, 0.2$  and  $0.3$ , respectively in Fig. 8b–d. These reduced magnetic moments are in agreement with the subdued ferromagnetic interaction from the M–T curves. Inset of Fig. 7 shows the inverse susceptibility ( $\chi^{-1}$ ), whose data in the higher temperature range (from 300 to 100 K) can be well fitted by the modified Curie-Weiss law [23]:

$$\chi = \chi_0 + \frac{C}{T - \theta}$$

where  $\chi_0$  denotes the temperature-independent term,  $C$  is the Curie constant and  $\theta$  is the paramagnetic Curie temperature. From the equation  $\mu_{eff} = \sqrt{8C} \mu_B$ , the effective magnetic moments of Co were calculated. The obtained  $\mu_{eff}$  values are 2.48, 2.59, 2.64 and 2.95  $\mu_B/Co$  for nominal  $x = 0, 0.1, 0.2$  and  $0.3$ , respectively. Compared with that of  $Co^{2+}$  ion (3.87  $\mu_B$ ), the effective magnetic moments of Co in all  $K_{1-x}Co_2Se_2$  samples are smaller, indicating the itinerant magnetism nature in these phases.

Combining the lattice parameters obtained from the refinements, it is interesting to find that the ferromagnetic interaction is weakened with the K vacancies induced, despite the Co-Co distance in  $ab$  plane (equal to  $\frac{\sqrt{2}}{2}a$ ) is obviously shortened from 2.746 to 2.695 Å with  $x$  changed from 0 to 0.3. In general, the magnetic interaction in layered Co-based materials should be highly related to the Co-Co distance in  $ab$  plane, where the shorter Co-Co distance usually leads to stronger interaction with higher critical temperature (Neel temperature  $T_N$  or  $T_C$ ). However, previous literatures reported the higher  $T_C$  combined with longer Co-Co distance in some Co-based phosphides ( $La_{1-x}Pr_xCo_2P_2$ ,  $LaCo_{2-x}Fe_xP_2$ , etc.) [37,38], which suggested that the magnetic interaction in these materials could be dominated by the electron structure rather than the crystal structure parameters.  $K_{1-x}Co_2Se_2$  presented here further confirms this feature that the magnetic interaction is mainly determined by carrier concentration instead of the Co-Co distance in  $ab$  plane. Meanwhile the evidence in our work is even stronger than the reported systems since no foreign element is involved in  $K_{1-x}Co_2Se_2$  but only the K deficiency induced, unlike the  $La_{1-x}Pr_xCo_2P_2$  or  $LaCo_{2-x}Fe_xP_2$  systems with foreign species doped. This novel phenomenon in Co-based 122-type materials could be attributed to their itinerant magnetism nature, which is confirmed by the calculations that we will show below.

In order to understand the mechanism of the decline on ferromagnetic ordering in  $K_{1-x}Co_2Se_2$  with the increased K vacancies, first-principles calculation was carried out to calculate the electronic structure of  $KCo_2Se_2$  and nonstoichiometric  $K_{0.75}Co_2Se_2$  (it is convenient to induce 25% K deficiency in the structural model). As shown in Fig. 9, both compounds exhibit metallic state with the density of states (DOS) crossing the Fermi level, in accordance with the observed metallic behavior in Fig. 6. Calculation on spin-polarized partial DOS shows that the majority DOS near the Fermi level are contributed by Co atoms (red curves in Fig. 9a and b). The magnetic moment for  $KCo_2Se_2$  is calculated to be 2.29  $\mu_B/Co$  (consistent with the reported calculation [39]), and this value is significantly reduced to 1.72  $\mu_B/Co$  for K deficient  $K_{0.75}Co_2Se_2$ , implying the degenerative magnetic interaction. The integral difference between the spin-up and spin-down DOS channels crossing the Fermi level is 1.27 states/eV·Co for  $KCo_2Se_2$  and this value falls to 0.90 for  $K_{0.75}Co_2Se_2$  as shown in Fig. 9c, mainly attributed to the reduced carrier concentration from the K vacancies. These results unambiguously indicate that the ferromagnetic interaction in K-deficient  $K_{0.75}Co_2Se_2$  is weakened, compared with that of vacancy-free  $KCo_2Se_2$ . In consequence, we declare that in  $K_{1-x}Co_2Se_2$  system, the charge transfer from intermediate metal K, which determines the charge transfer to [CoSe] host layers, plays a more crucial role to regulate the magnetism.

It is worth noting that an anomaly is also observed at 14 K in the M–T curve of sample  $x = 0.3$  (Fig. 7), which may be resulted from another magnetic transition in lower temperature range. As reported in literature, stoichiometric  $KCo_2Se_2$  shows A-type ferromagnetic ordering

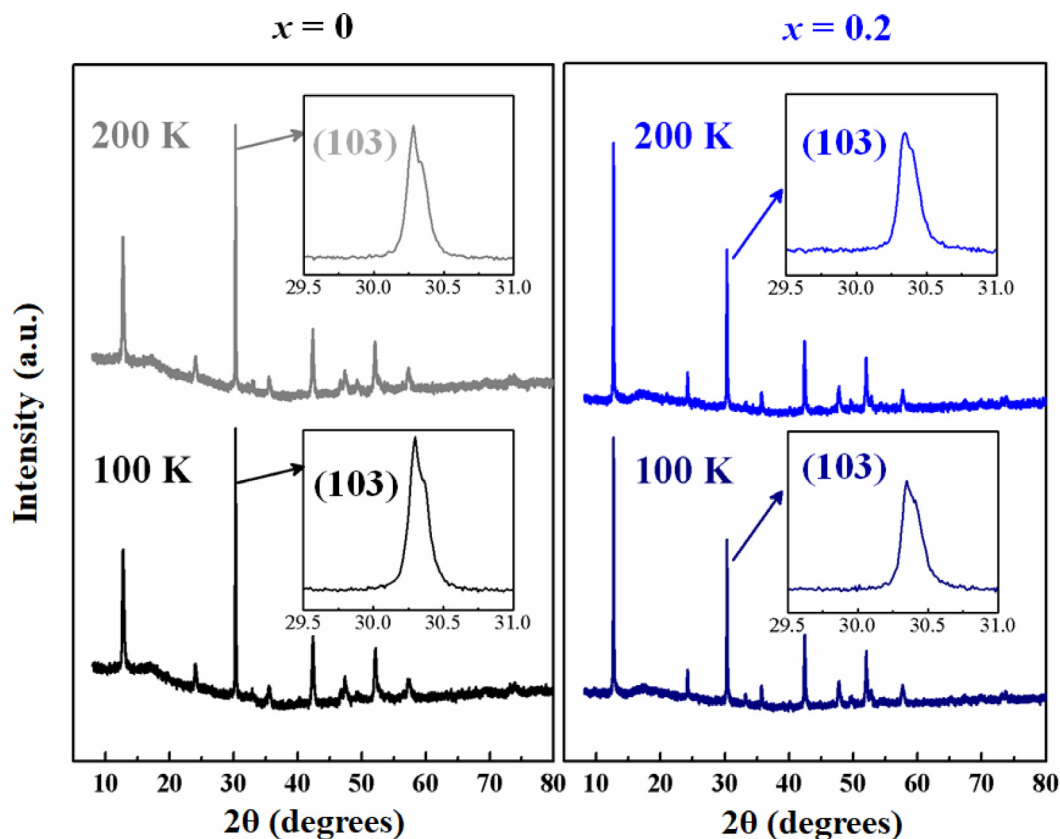


Fig. 5. In situ PXRD patterns for sample  $x = 0$  and  $0.2$  at  $200$  and  $100$  K. Inset shows the enlarged  $(103)$  diffraction peaks in the patterns.

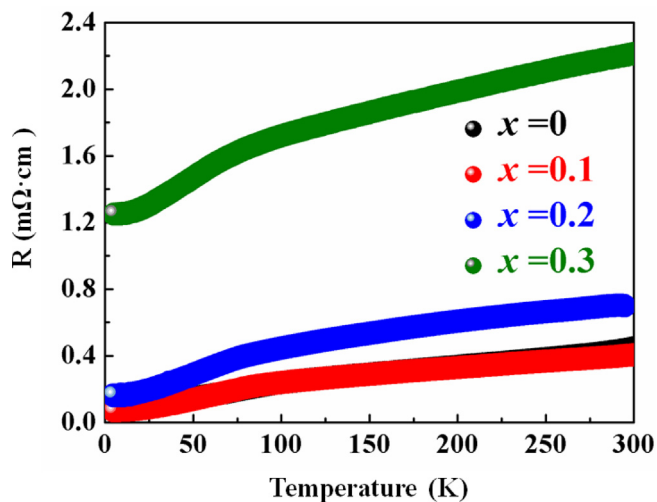


Fig. 6. Temperature-dependent resistivity of nominal  $K_{1-x}Co_2Se_2$  with  $x = 0, 0.1, 0.2$  and  $0.3$ .

with the magnetic moment of Co parallel to the  $ab$  plane. As the K vacancies induced, a modulation on the original magnetic structure may occur. Additionally, Zhou et al., reported the synthesis of tetragonal CoSe by de-intercalating the potassium from  $KCo_2Se_2$  and suggested at first that CoSe is ferromagnetic [33]. Later, their colleagues Wilfong et al., demonstrated the frustrated magnetic ordering instead (spin-glass state) in tetragonal CoSe by more systematic magnetic representation [40]. In  $K_{0.7}Co_2Se_2$  with  $\sim 30\%$  K deficiency, the ferromagnetic interaction may also be frustrated, resulting in the anomaly in both  $M-T$  and  $M-H$  curves (Figs. 7 and 8d). Further investigation should be done in future using more accurate characterization (such as

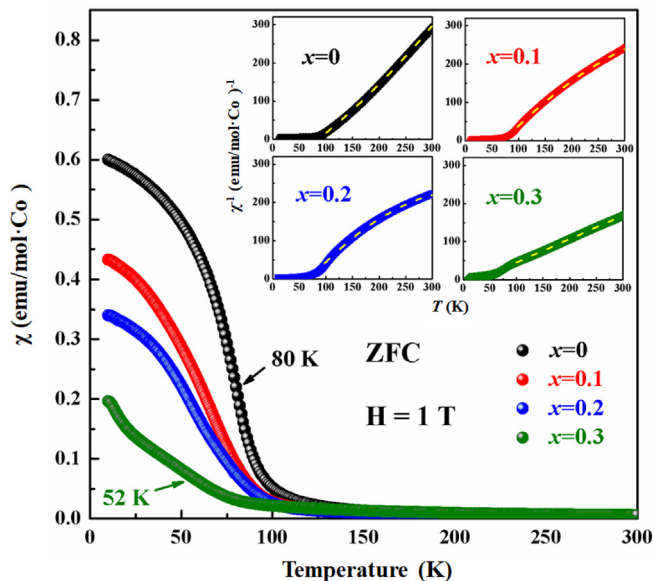


Fig. 7. Temperature-dependence of magnetic susceptibility of  $K_{1-x}Co_2Se_2$  with  $x = 0, 0.1, 0.2$  and  $0.3$  under the field of  $H = 1$  T with zero-field cooling (ZFC). Inset shows the inverse of susceptibility versus temperature with the modified Curie-Weiss fitting (dash yellow lines). (For interpretation of the references to colour in this figure legend, the reader is referred to the web version of this article.)

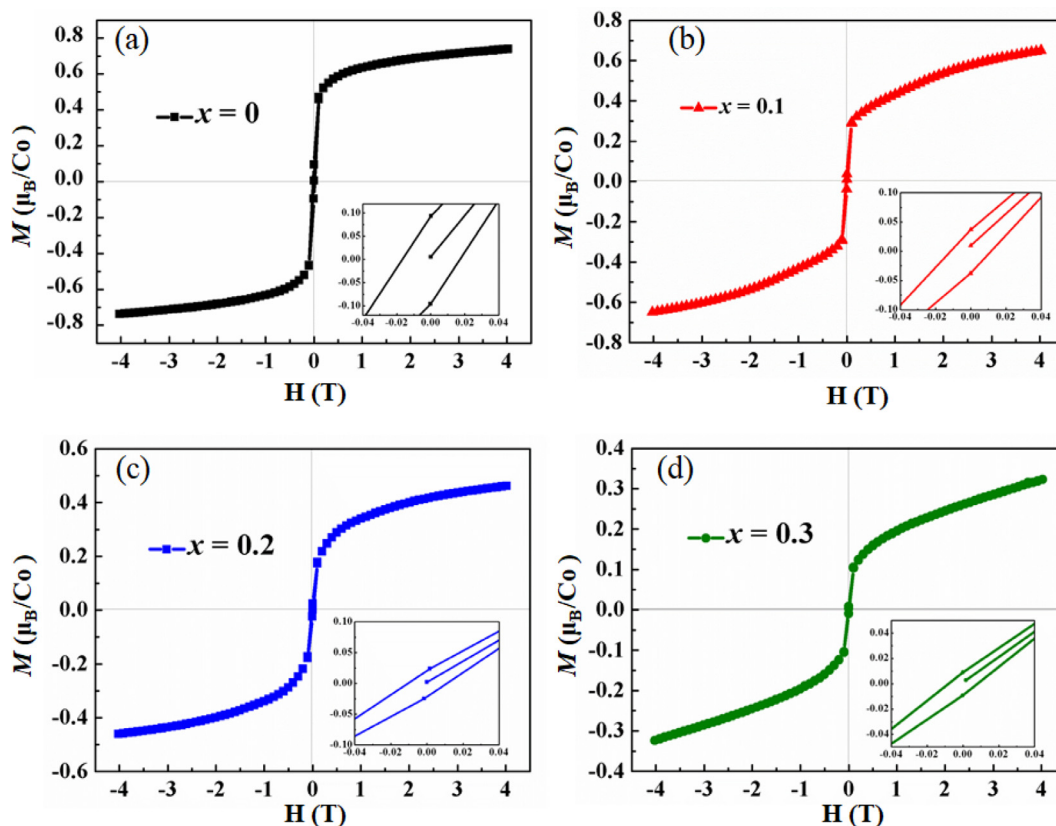


Fig. 8. Hysteresis loops for  $\text{K}_{1-x}\text{Co}_2\text{Se}_2$  at 10 K with (a)  $x = 0$ , (b)  $x = 0.1$ , (c)  $x = 0.2$ , and (d)  $x = 0.3$ . Inset shows the enlarged curves near the coordinate zero point, indicating the weak hysteresis in all four samples.

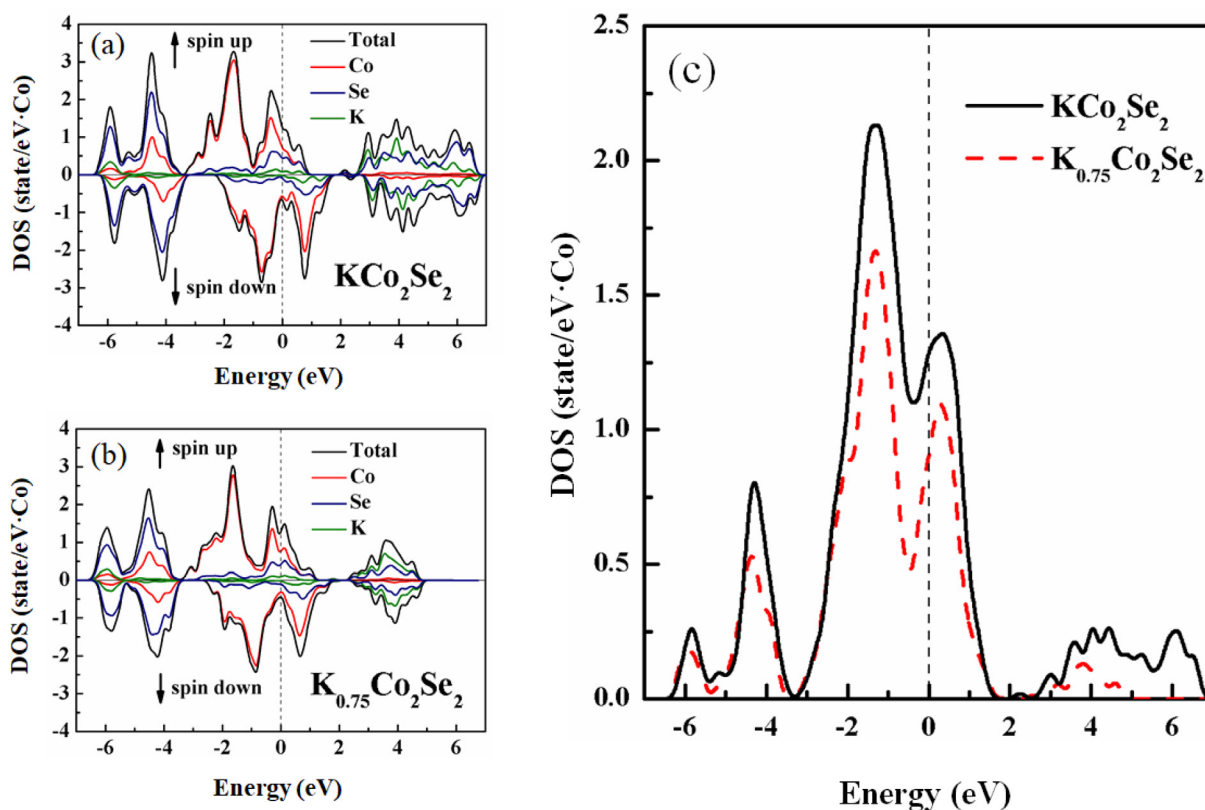


Fig. 9. Spin-polarized partial DOS for (a)  $\text{KCo}_2\text{Se}_2$  and (b)  $\text{K}_{0.75}\text{Co}_2\text{Se}_2$ . (c) Integral difference between the spin-up and spin-down DOS of  $\text{KCo}_2\text{Se}_2$  and  $\text{K}_{0.75}\text{Co}_2\text{Se}_2$ . The dash line is the Fermi level.

neutron powder diffraction) to determine the magnetic structure of  $K_{0.7}Co_2Se_2$  sample at low temperature.

#### 4. Conclusions

In conclusion, a series of  $K_{1-x}Co_2Se_2$  was successfully synthesized by solid state reaction and the tunable K vacancies (up to ~30%) were demonstrated in this system via analyzing the chemical composition and structural parameters. We exclude the existence of Co deficiency from refinements and EDS, suggesting the intact [CoSe] functional layers can be maintained with the K vacancies regulated in this system. Based on the controllable K vacancies in this  $ThCr_2Si_2$ -type compound, the structure parameters and related properties can be effectively adjusted. By inducing the K vacancies, the lattice constant  $a$  is compressed while  $c$  is enlarged, resulting in an increased  $c/a$  ratio. The distortion of  $CoSe_4$  tetrahedron is also intensified resulted from the deficient K in the structure. Although the oxide state of Co is basically unchanged, the K vacancies raise the electric resistivity and most importantly, regulate the strength of ferromagnetic interaction in this layered Co selenide with Curie temperature  $T_C$  varying from 80 to 52 K. First-principles calculation shows that this regulation on magnetism is mainly attributed to the modulation of charge transfer from the intermediate metal K to [CoSe] host layers. Our results not only offer a reliable route to regulate the structure and electromagnetic properties of  $ATM_2X_2$  materials, but also address the important interplay between the charge transfer and magnetic interaction in  $ThCr_2Si_2$ -type materials.

#### Acknowledgements

We would like to thank Chen X.L. and Jin S.F. from Institute of Physics, Chinese Academy of Sciences for the useful discussion. The financial supports by the National Natural Science Foundation of China (No. 51532010, 51872028 and 51832010) and the Fundamental Research Funds for the Central Universities (FRF-BR-18-009B) are gratefully acknowledged.

#### Conflicts of interest

The authors declare no competing financial interest.

#### References

- [1] P. Villars, International, A Pearson's Handbook of Crystallographic Data for Intermetallic Phases, 2nd ed., ASM International, Novlety, OH, 1991.
- [2] X.Q. Zhou, E.E. Rodriguez, Tetrahedral transition metal chalcogenides as functional inorganic materials, *Chem. Mater.* 29 (2017) 5737–5752.
- [3] Z. Guo, F. Sun, W. Yuan, Chemical intercalations in layered transition metal chalcogenides: syntheses, structures, and related properties, *Cryst. Growth Des.* 17 (2017) 2238–2253.
- [4] J. Paglione, R.L. Greene, High-temperature superconductivity in iron-based materials, *Nature Phys.* 6 (2010) 645–658.
- [5] J. Guo, S. Jin, G. Wang, S. Wang, K. Zhu, T. Zhou, M. He, X. Chen, Superconductivity in the iron selenide  $K_xFe_2Se_2$  ( $0 \leq x \leq 1.0$ ), *Phys. Rev. B* 82 (2010) 180520.
- [6] G. Huan, M. Greenblatt, M. Croft, New ternary transition metal chalcogenides  $AM_2X_2$  ( $A = K, Rb, Cs; M = Co; A = K, M = Ni; X = S, Se$ ): magnetically ordered metals with the  $ThCr_2Si_2$ -type structure, *Eur. J. Solid State Inorg. Chem.* 26 (1989) 193–220.
- [7] J.R. Neilson, A. Llobet, A.V. Stier, L. Wu, J. Wen, J. Tao, Y. Zhu, Z.B. Tesanovic, N.P. Armitage, T.M. McQueen, Mixed-valence-driven heavy-fermion behavior and superconductivity in  $KNi_2Se_2$ , *Phys. Rev. B* 86 (2012) 054512.
- [8] T.P. Ying, X.L. Chen, G. Wang, S.F. Jin, T.T. Zhou, X.F. Lai, H. Zhang, W.Y. Wang, Observation of superconductivity at 30–46 K in  $A_xFe_2Se_2$  ( $A = Li, Na, Ba, Sr, Ca, Yb$ , and  $Eu$ ), *Sci. Rep.* 2 (2012) 426.
- [9] T. Ying, X. Chen, G. Wang, S. Jin, X. Lai, T. Zhou, H. Zhang, S. Shen, W. Wang, Superconducting phases in potassium-intercalated iron selenides, *J. Am. Chem. Soc.* 135 (2013) 2951–2954.
- [10] S. Jin, X. Fan, X. Wu, R. Sun, H. Wu, Q. Huang, C. Shi, X. Xi, Z. Li, X. Chen, High- $T_c$  superconducting phases in organic molecular intercalated iron selenides: synthesis and crystal structures, *Chem. Commun.* 53 (2017) 9729–9732.
- [11] K. Kovnir, W.M. Reiff, A.P. Menushenkov, A.A. Yaroslavtsev, R.V. Chernikov, M. Shatruk, “Chemical Metamagnetism”: from antiferromagnetic  $PrCo_2P_2$  to ferromagnetic  $Pr_{0.8}Eu_{0.2}Co_2P_2$  via chemical compression, *Chem. Mater.* 23 (2011) 3021–3024.

- [12] C.M. Thompson, X. Tan, K. Kovnir, V.O. Garlea, A.A. Gippius, A.A. Yaroslavtsev, A.P. Menushenkov, R.V. Chernikov, N. Büttgen, W. Kratschmer, Y.V. Zubavichus, M. Shatruk, Synthesis, structures and magnetic properties of rare-earth cobalt arsenides,  $RCo_2As_2$  ( $R = La, Ce, Pr, Nd$ ), *Chem. Mater.* 26 (2014) 3825–3837.
- [13] X. Tan, G. Fabbri, D. Haskel, A.A. Yaroslavtsev, H. Cao, C.M. Thompson, K. Kovnir, A.P. Menushenkov, R.V. Chernikov, V.O. Garlea, M. Shatruk, A transition from localized to strongly correlated electron behavior and mixed valence driven by physical or chemical pressure in  $ACo_2As_2$  ( $A = Eu$  and  $Ca$ ), *J. Am. Chem. Soc.* 138 (2016) 2724–2731.
- [14] X. Tan, A.A. Yaroslavtsev, H. Cao, A.Y. Geondzhian, A.P. Menushenkov, R.V. Chernikov, L. Nataf, V.O. Garlea, M. Shatruk, Controlling magnetic ordering in  $Ca_{1-x}Eu_xCo_2As_2$  by chemical compression, *Chem. Mater.* 28 (2016) 7459–7469.
- [15] S. Shen, G. Wang, S. Jin, Q. Huang, T. Ying, D. Li, X. Lai, T. Zhou, H. Zhang, Z. Lin, X. Wu, X. Chen, Tunable cobalt vacancies and related properties in  $LaCo_2As_2$ , *Chem. Mater.* 26 (2014) 6221–6225.
- [16] Z. Guo, F. Sun, B. Han, K. Lin, L. Zhou, W. Yuan, Iron vacancy in tetragonal  $Fe_{1-x}S$  crystals and its effect on the structure and superconductivity, *Phys. Chem. Chem. Phys.* 19 (2017) 9000–9006.
- [17] C.M. Thompson, K. Kovnir, S. Eveland, M.J. Herring, M. Shatruk, Synthesis of  $ThCr_2Si_2$ -type arsenides from Bi flux, *Chem. Commun.* 47 (2011) 5563–5565.
- [18] P.L. Alireza, Y.T. Chris Ko, J. Gillett, C.M. Petrone, J.M. Cole, G.G. Lonzarich, S.E. Sebastian, Superconductivity up to 29 K in  $SrFe_2As_2$  and  $BaFe_2As_2$  at high pressures, *J. Phys.: Condens. Matter* 21 (2009) 012208.
- [19] J.R. Neilson, T.M. McQueen, Bonding, ion mobility, and rate-limiting steps in deintercalation reactions with  $ThCr_2Si_2$ -type  $KNi_2Se_2$ , *J. Am. Chem. Soc.* 134 (2012) 7750–7757.
- [20] G. Huan, M. Greenblatt, Antiferromagnetic-to-ferromagnetic transition in metallic  $Tl_{1-x}K_xCo_2Se_2$  ( $0 \leq x \leq 1.0$ ) with  $ThCr_2Si_2$ -type structure, *J. Less-Common Met.* 156 (1989) 247–257.
- [21] A. Broddefalk, P. Nordblad, R. Berger, Structural and magnetic properties of  $TlCo_2-xCu_xSe_2$ ,  $0 \leq x \leq 1$ , *Physica B* 284–288 (2000) 1317–1318.
- [22] S. Ronneterg, R. Berger, R.Z. Levitin, E.A. Popova, R.M. Scherbov, A.N. Vasiliev, Longitudinal spin fluctuations in thermal and magnetic properties of  $TlCo_2Se_2-xS_x$ , *J. Magn. Magn. Mater.* 281 (2004) 388–393.
- [23] J. Yang, B. Chen, H. Wang, Q. Mao, M. Imai, K. Yoshimura, M. Fang, Magnetic properties in layered  $ACo_2Se_2$  ( $A = K, Rb, Cs$ ) with the  $ThCr_2Si_2$ -type structure, *Phys. Rev. B* 88 (2013) 064406.
- [24] Z. Guo, H. Zhang, D. Wang, B. Han, S. Jin, W. Yuan, Ferromagnetic interlayer interaction in  $KCo_2Se_2-xS_x$  ( $0 \leq x \leq 2$ ) and its chemical origin, *Dalton Trans.* 45 (2016) 8248–8252.
- [25] J. Yang, W. Yang, Q. Zhu, B. Chen, H. Wang, Q. Mao, J. Du, Z. Lou, M. Fang, Spin-flop transition and magnetic phase diagram in  $CsCo_2Se_2$  revealed by torque and resistivity measurements, *J. Magn. Magn. Mater.* 474 (2019) 70–75.
- [26] J. Rodriguez-Carvajal, Recent advances in magnetic structure determination by neutron powder diffraction, *Phys. B* 192 (1993) 55–69.
- [27] J.P. Perdew, K. Burke, M. Ernzerhof, Generalized gradient approximation made simple, *Phys. Rev. Lett.* 77 (1996) 3865–3868.
- [28] H.J. Monkhorst, J.D. Pack, Special points for Brillouin-zone integrations, *Phys. Rev. B* 13 (1976) 5188–5192.
- [29] J.W. Kim, S.M. Park, In situ XANES studies of electrodeposited nickel oxide films with metal additives for the electro-oxidation of ethanol, *J. Electrochem. Soc.* 150 (2003) E560–E566.
- [30] C. Roux, D.M. Adams, J.P. Itié, A. Polian, D.N. Hendrickson, M. Verdagner, Pressure-induced valence tautomerism in cobalt o-quinone complexes: an X-ray absorption study of the low-spin  $[Co^{III}(3,5-DTBSQ)(3,5-DTBCat)(phen)]$  to high-spin  $[Co^{II}(3,5-DTBSQ)_2(phen)]$  interconversion, *Inorg. Chem.* 35 (1996) 2846–2852.
- [31] M.O. Figueiredo, T.P. Silva, J.P. Veiga, A XANES study of cobalt speciation state in blue-and-white glazes from 16<sup>th</sup> to 17<sup>th</sup> century Chinese porcelains, *J. Electron. Spectrosc. (Related Phenomena)* 185 (2012) 97–102.
- [32] G. Jacobs, P.M. Patterson, T.K. Das, M. Luo, B.H. Davis, Fischer-Tropsch synthesis: effect of water on  $Co/Al_2O_3$  catalysts and XAFS characterization of reoxidation phenomena, *Appl. Catal. A-Gen.* 270 (2004) 65–76.
- [33] X. Zhou, B. Wilfong, H. Vivanco, J. Paglione, C.M. Brown, E.E. Rodriguez, Metastable layered cobalt chalcogenides from topochemical deintercalation, *J. Am. Chem. Soc.* 138 (2016) 16432–16442.
- [34] Z. Guo, L. Zhou, S. Jin, B. Han, F. Sun, W. Yuan,  $K_x(C_2H_8N_2)_yFe_{2-z}S_2$ : synthesis, phase structure and correlation between  $K^+$  intercalation and Fe depletion, *RSC Adv.* 7 (2017) 17539–17544.
- [35] After de-intercalation of K in  $KCo_2Se_2$ , the  $(CoSe_4)$  tetrahedrons could be remained, but the binary CoSe shows a n-glide along ab plane from  $ThCr_2Si_2$ -type, forming the anti-PbO structure with P4/nmm space group. So the lattice parameters of binary CoSe reported by Zhou et al., (Ref. 33) are not plotted in Fig. 4 in this work for comparison.
- [36] A. Sobhani, M. Salavati-Niasari, Cobalt selenide nanostructures: hydrothermal synthesis, considering the magnetic property and effect of the different synthesis conditions, *J. Mol. Liq.* 219 (2016) 1089–1094.
- [37] K. Kovnir, C.M. Thompson, H.D. Zhou, C.R. Wiebe, M. Shatruk, Tuning ferro- and metamagnetic transitions in rare-earth cobalt phosphides  $La_{1-x}Pr_xCo_2P_2$ , *Chem. Mater.* 22 (2010) 1704–1713.
- [38] K. Kovnir, V.O. Garlea, C.M. Thompson, H.D. Zhou, W.M. Reiff, A. Ozarowski, M. Shatruk, Spin-glass behavior in  $LaFe_xCo_{2-x}P_2$  solid solutions: interplay between magnetic properties and crystal and electronic structures, *Inorg. Chem.* 50 (2011) 10274–10283.
- [39] V.V. Bannikov, I.R. Shein, A.L. Ivanovskii, Structural, electronic, magnetic and elastic properties of tetragonal layered diselenide  $KCo_2Se_2$  from first principles calculations, *Physica B* 407 (2012) 271–275.
- [40] B. Wilfong, X. Zhou, H. Vivanco, D.J. Campbell, K. Wang, D. Graf, J. Paglione, E. Rodriguez, Frustrated magnetism in the tetragonal CoSe analog of superconducting FeSe, *Phys. Rev. B* 97 (2018) 104408.